LAWRENCE
LIVERMORE
NATIONAL
LABORATORY

LLNL-TR-687901

Attenuation Drift in the Micro-Computed Tomography System at LLNL

A. A. Dooraghi, W. Brown, I. Seetho, J. Kallman, K. Lennox, L. Glascoe, H. Martz

April 5, 2016

Disclaimer

This work performed under the auspices of the U.S. Department of Energy by Lawrence Livermore National Laboratory under Contract DE-AC52-07NA27344.

Attenuation Drift in the Micro-Computed Tomography System at LLNL

Alex Dooraghi, Bill Brown, Isaac Seetho, Jeff Kallman, Kristin Lennox, Lee Glascoe

January 12, 2016

Executive Summary

The maximum allowable level of drift in the linear attenuation coefficients (μ) for a Lawrence Livermore National Laboratory (LLNL) micro-computed tomography (MCT) system was determined to be 0.1%. After ~100 scans were acquired during the period of November 2014 to March 2015, the drift in μ for a set of six reference materials reached or exceeded 0.1%. Two strategies have been identified to account for or correct the drift. First, normalizing the 160 kV and 100 kV μ data by the μ of water at the corresponding energy, in contrast to conducting normalization at the 160 kV energy only, significantly compensates for measurement drift. Even after the modified normalization, μ of polytetrafluoroethylene (PTFE) increases linearly with scan number at an average rate of 0.00147% per scan. This is consistent with PTFE radiation damage documented in the literature. The second strategy suggested is the replacement of the PTFE reference with fluorinated ethylene propylene (FEP), which has the same effective atomic number (Z_e) and electron density (ρ_e) as PTFE, but is 10 times more radiation resistant. This is important as effective atomic number and electron density are key parameters in analysis. The presence of a material with properties such as PTFE, when taken together with the remaining references, allows for a broad range of the (Z_e, ρ_e) feature space to be used in analysis. While FEP is documented as 10 times more radiation resistant, testing will be necessary to assess how often, if necessary, FEP will need to be replaced. As radiation damage to references has been observed, it will be necessary to monitor all reference materials for radiation damage to ensure consistent x-ray characteristics of the references.

1. Introduction[1]

Micro-computed tomography (MCT) is a high resolution radiographic technique used for the non-destructive, three-dimensional characterization of small objects. Multiple radiographs of an object are taken from different angles, and reconstruction algorithms are used to determine the properties of the specimen. In the MCT system at Lawrence Livermore National Laboratory (LLNL), a carousel is used to position the specimen of interest as well as reference materials required for analysis. Figure 1 shows a diagram and photo of the LLNL MCT machine. For this particular setup, x-rays emitted from the source pass through a two-slit collimator. The top slit allows x-rays to pass through a test

[1] Much of the background information in this section was taken from "A Bayesian Measurement Error Model for Misaligned Radiographic Data" by Kristin Lennox and Lee Glascoe. The article was published in Volume 55 of *Technometrics*, pp 450-460 (2013).

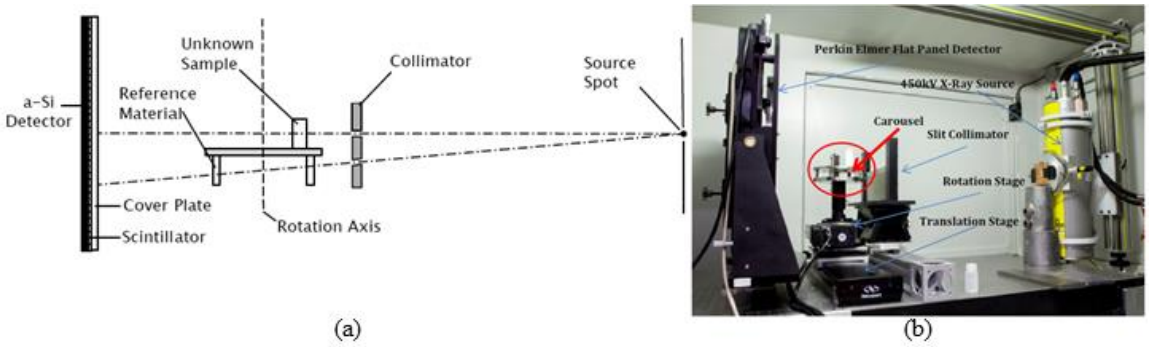

Figure 1 (a) Diagram and (b) photo of MCT system configuration at LLNL.

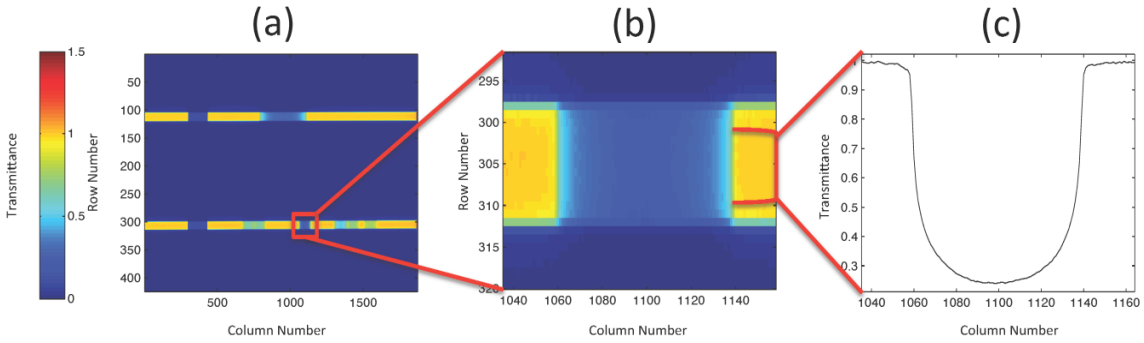

Figure 2 The process of converting a radiograph into a lineout for the aluminum reference specimen. Note the copper strip on far left in (a). These images show transmittance measurements.

specimen, while the lower slit gives access to a set of six reference materials. These reference materials are included in every MCT run for quality control purposes. Unabsorbed x-rays are registered by an amorphous silicon detector. Specimen and reference materials are attached to a carousel, which rotates in increments of half a degree to give 720 different views per experimental run.

Figure 2 shows a representative transmission radiograph. Figure 2a is the measured transmittance at every pixel of the detector. Transmittance is the ratio of the measured intensity at a particular pixel to the background intensity value corresponding to measured intensity when there is no intervening material.

Transmittance is close to 1 in regions where there is no intervening material between the source and the detector, and drops to 0 when the intervening material blocks all x-ray transmission. The two light horizontal bands correspond to the slits in the collimator between the source and the carousel. The darker vertical bands are caused by either the specimen of interest (top slit) or reference materials (lower slit). The darkest vertical band on the far left is a copper strip attached to the collimator for calibration purposes. Figure 2b shows the isolation of a single reference material, in this case an aluminum cylinder, from the larger radiograph. Figure 2c is a *lineout*, a one-dimensional summary of a radiograph that is in this case generated by the pointwise median from the central

Figure 3 A reconstructed slice showing reference materials. Defined region of interest ROIs are used to determine μ.

rows of the lower slit. Lineouts from multiple radiographs taken for different carousel positions can be used to generate 2-dimensional reconstructions, which are representations of a "slice" taken out of the core of the sample.

For a standard measurement, data is collected at x-ray energies of 100 kV and 160 kV. In addition to acquiring 720 projections at half degree increments, dark and background images are taken at the end of each scan in order to convert the raw projections into attenuation radiographs (attenrads). The dark radiograph ($\mathbf{R_{dark}}$) is an image taken at the same integration time as the raw radiographs ($\mathbf{R_{raw}}$) but with the x-ray source turned off. This frame is used to subtract the dark current signal. A background radiograph ($\mathbf{R_{bak}}$) is a radiograph taken with the x-ray source on and at the same integration time as the raw radiograph, but with no object between the source and the detector. The dark radiograph is subtracted from both the raw radiographs and the background radiograph in order to generate dark corrected raw radiographs and a dark corrected background radiograph. In order to account for differences in flux between the raw radiograph and the background radiograph a postage stamp region is used in the calculation of the attenrads. Hence, attenrads are generated as:

$$attenrad = -\ln\left(\left[\frac{\boldsymbol{R_{raw}} - \boldsymbol{R_{dark}}}{\boldsymbol{R_{bak}} - \boldsymbol{R_{dark}}}\right]\frac{s_o}{s}\right)$$

where s is the mean of an ROI unobstructed by objects in the dark corrected raw radiograph, and s_o is the mean of an ROI positioned as in s, but in the dark corrected background radiograph. Typically a reconstruction postage stamp is located on the upper strip for the purpose of normalizing for flux. The attenrads are then processed according to the fan beam filtered backprojection algorithm.

The objective is to determine the properties of a specimen by measuring the linear attenuation coefficient (μ) of the reference materials and specimen at these two x-ray source energies (Brown and Smith, 2013). After reconstruction, μ values of the references acquired with both source settings are recorded using defined regions of interest extracted through a technique call active contour (Seetho et al., 2011) (Figure 3).

Measured μ values are generally reported in Livermore Modified Hounsfield Units (LMHU), which are normalized such that the 160 kV measurement of the water reference specimen has a value of 1000. That normalization factor is then applied to the 100 kV data.

The LLNL team has noted a drift in μ for the standard set of reference materials: graphite, water, silicon, magnesium, polyoxymethylene (trade name Delrin), and polytetrafluoroethylene (PTFE)[2]. Consequently, current program objectives are to (1) understand the observed drift and its causes, and (2) correct the drift or minimize its effect. To date, effort in correcting or accounting for this drift has yielded the following promising avenues:

(1) Normalizing the 160 kV and 100 kV μ data by the μ of the water reference at the corresponding energy significantly compensates for drift.
(2) Even after normalization, μ of PTFE increases with scan number. A literature review revealed that PTFE is vulnerable to radiation damage that is consistent with the observed drift, and therefore a replacement reference material should be considered.

Some analysis has also been carried out for the Cu strip and postage stamp regions, which may eventually lead to further recommendations.

Section 2 will describe the observed drift. Sections 3-6 will describe in detail the abovementioned efforts to account or correct for this drift.

2. Identification of drift

Assessment of μ began after ~100 scans were acquired. Acquisition spanned the period of November 2014 to March 2015. Figure 4 shows the percent change of μ from the first recorded scan at x-ray peak energies of 100 kV and 160 kV. For a given material and peak x-ray energy, the percent change of μ was calculated as:

$$Percent\ Change\ of\ \mu = \frac{\mu - \mu_o}{\mu_o} x100\%$$

where μ_o is the linear attenuation coefficient of the first scan. The percent change of μ at 160 kV tracks well with that at 100 kV for roughly the first 20 scans, after which the percent change of μ at 160 kV increases markedly. A threshold of 0.1% was

[2] Polytetrafluoroethylene (PTFE) is a synthetic fluoropolymer commonly known by the Dupont commercial name, Teflon (PTFE).

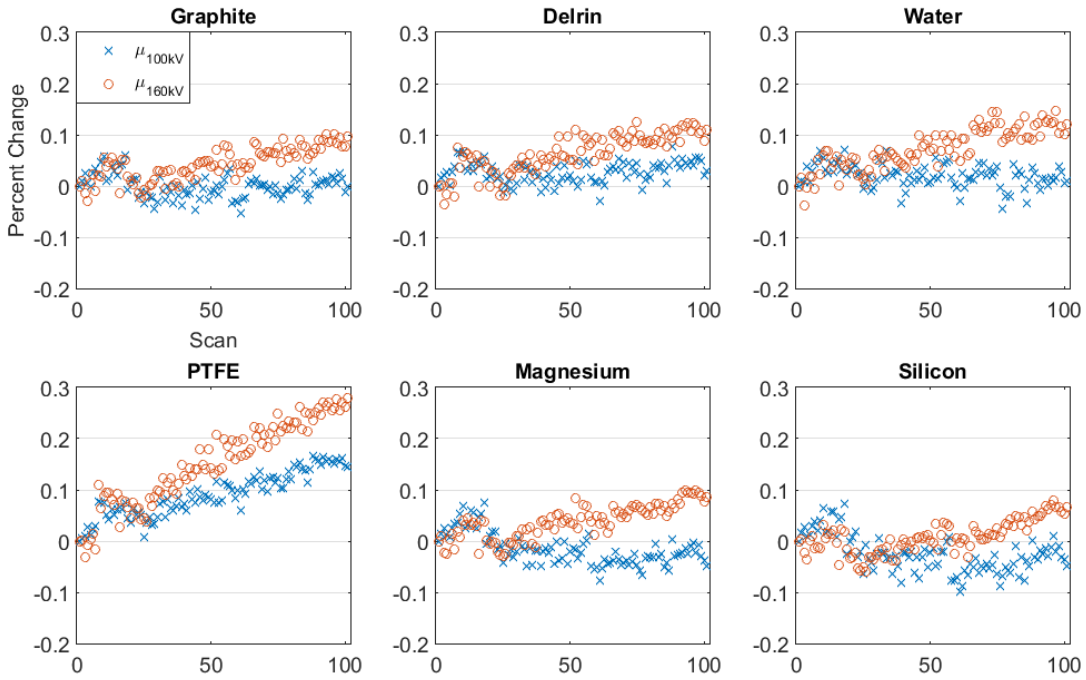

Figure 4 The percent change of μ (un-normalized data) from the first scan at both 100 kV and 160 kV.

calculated for allowable variation in μ[3]. For all reference materials, the percent change of μ for scans acquired at 160 kV approaches or exceeds 0.1 %. PTFE demonstrates a noticeably higher drift in μ for scans taken at both energy levels. PTFE at 160 kV reaches ~0.3% drift after 100 scans, which is more than double the rate of change for other materials.

Similarities between trends in reference materials suggest that a significant contribution of the drift at 160 kV is correlated between the reference materials. This shared pattern of drift suggests that this contribution to drift is due to a system component (source, detector, etc.). The unique trend displayed by PTFE suggests that on top of system drift, PTFE may be experiencing a secondary effect indicative of radiation damage. Correlated drift is explored in Section 3 via normalization to water. Radiation induced damage to PTFE is explored in Section 4.

[3] Threshold of 0.1% was calculated by examining the variation from 30 samples and determining a 95% confidence interval that a measurement is in agreement with the observed variability

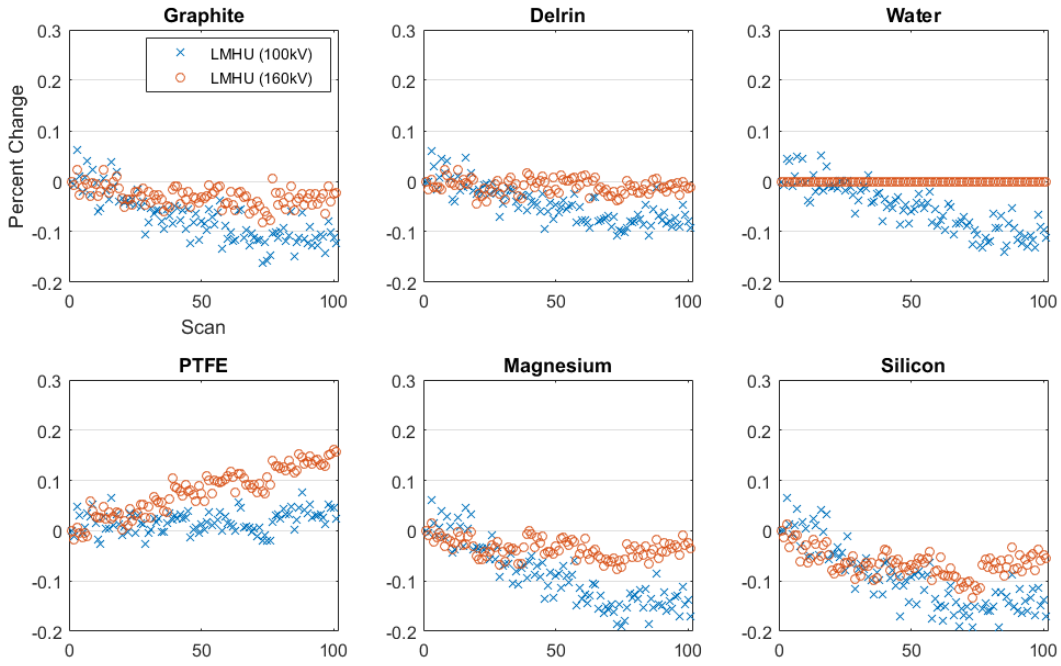

Figure 5 The percent change of LMHU calculated for the current normalization which uses the μ of water at 160 kV to normalize both energy sets.

3. Normalization by Water

The current normalization method uses the μ of water at 160 kV to normalize both the 100 kV and 160 kV data to create Livermore Modified Hounsfield Units (LMHU). Figure 5 shows the percent change of LMHU calculated for the current normalization. As shown in Figure 5, this normalization results in a percent change of the LMHU at 100 kV that approaches or exceed 0.1% for all references after ~100 scans.

In order to reduce the effect of the contribution to drift that is correlated between the reference materials, μ of water (μ_{water}) at both 100 kV and 160 kV were used to normalize the remaining reference material μ values ($\mu^* = \mu / \mu_{water}$). This method yields improved results as compared to normalization at one energy. Normalization by the linear attenuation coefficient of water at a given energy is a standard method in the medical field when analyzing dual energy CT data in order to reduce the effect of system drift (Johnson et al., 2007). Figure 6 shows percent change of μ^*. The μ^* at 100 kV and 160kV track well with each other. Of particular importance is the ratio of the linear attenuation coefficient acquired at 100 kV to 160 kV. Figure 7 shows percent change from the first recorded scan of the ratio for 100 scans. Normalization to water at the same energy level was also assessed and recommended in Lennox et al. (2014) when evaluating a previous configuration of the MCT system that utilized a Thales detector.

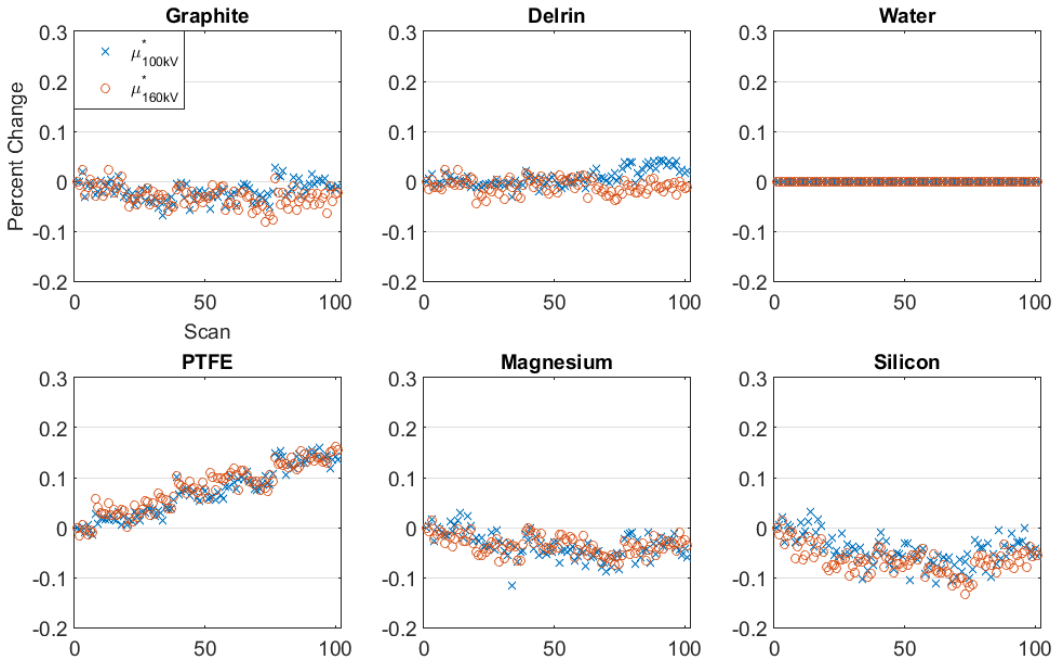

Figure 6 The percent change of μ^* from the first scan at both 100 kV and 160 kV.

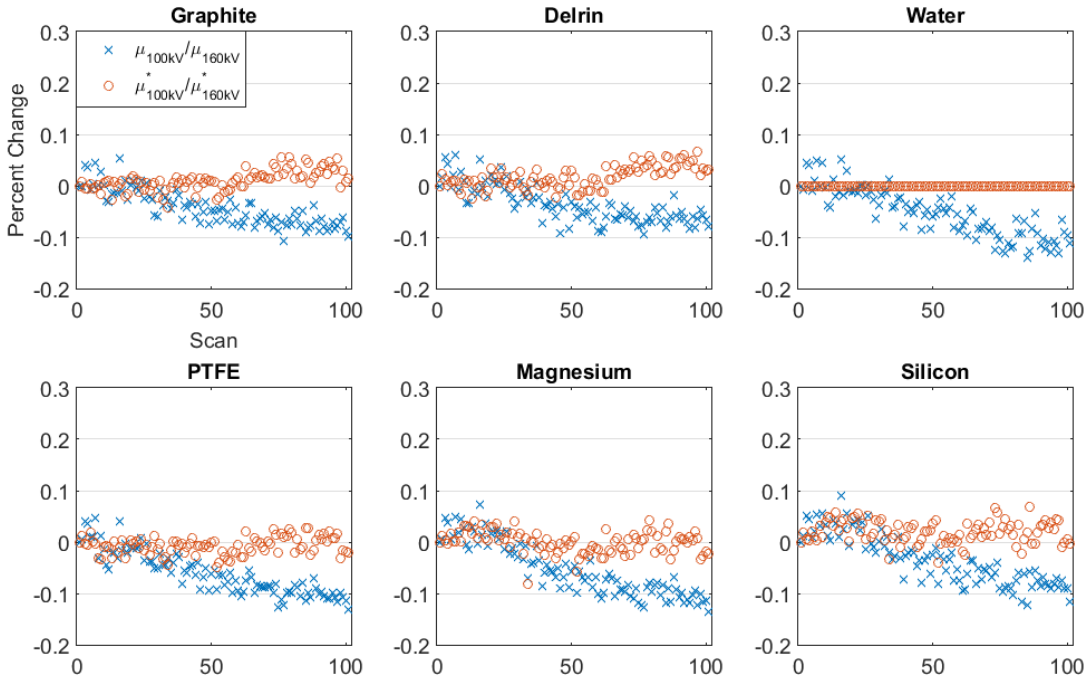

Figure 7 The percent change of μ_{100kV}/μ_{160kV} and $\mu^*_{100kV}/\ \mu^*_{160kV}$ as a function of scan number

4. Radiation Damage to PTFE

As previously mentioned, the plots of μ^* at 100 kV (μ^*_{100kV}) and μ^* at 160 kV (μ^*_{160kV}) of PTFE show a distinct slope even after normalization to water. On average the rate of change of μ^*_{100kV} and μ^*_{160kV} of PTFE is 0.00147% per scan. Studies have shown that PTFE undergoes compositional changes when exposed to radiation. Nishioka et al. (1959) propose that highly irradiated PTFE suffers a decrease in molecular weight which promotes a crystallization effect. To assess the effect on μ for PTFE from progressive radiation damage, the following examination was performed. To serve as a control, three CT scans were performed with a sample of PTFE from the MCT Test Bed which had been exposed to minimal radiation compared to the PTFE reference in question (scans 104-106). Subsequently, 21 scans were performed with the original piece of PTFE in a flipped orientation, such that the measured material had been subjected to minimal prior radiation exposure. Three additional scans were then performed with the control PTFE. As illustrated in Figure 8, while μ^* of PTFE after 21 scans of the flipped reference sample does not change appreciably, there is a clear shift produced from simply changing the location of radiation interaction on the PTFE reference. The 21 scans taken were not sufficient to show the trend; however, the slope was clearly visible after 50 subsequent measurements.

To address potential radiation damage complication with PTFE, a different material has been identified, fluorinated ethylene propylene (FEP)[4], which has the same effective atomic number (Z_e) and electron density (ρ_e) as PTFE but is 10 times more radiation resistant (Sterigenics). This is beneficial as PTFE provides a valuable data point that, along with the other references, helps cover a broad range of the (Z_e, ρ_e) feature space used in analysis. While FEP is documented as 10 times more radiation resistant, testing will be necessary to assess how often, if necessary, FEP will need to be replaced.

[4] Fluorinated ethylene propylene or FEP is a copolymer of hexafluoropropylene and tetrafluoroethylene and is very similar in composition to PTFE.

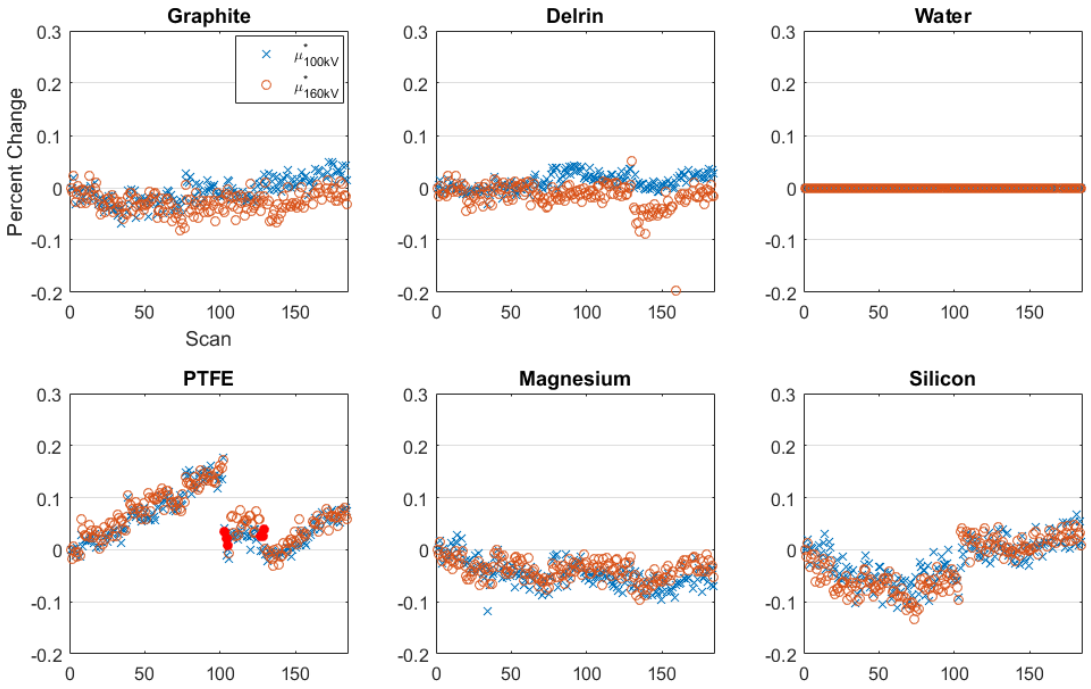

Figure 8 The percent change of the normalized linear attenuation coefficient from the first scan at both 100 kV and 160 kV. Solid red circles in PTFE plot represent the percent change of μ^*_{160kV} for the PTFE control material scans. PTFE sample was changed out for scans 104-106, original was flipped for scans 107-127, and again changed out for scans 128-130. After which, the original flipped sample was placed again and scanned an additional 50 times.

Figure 9 Sample raw radiograph illustrating location of parameters used to calculate the Cu strip metric.

5. Evaluation of copper strip data

A copper (Cu) strip region is used to evaluate spectrum changes (Figure 2 and Figure 9). The Cu strip metric, $\mu_{Cu}L$, is calculated as:

$$\mu_{Cu}L = mean\left[-\ln\left(\frac{\boldsymbol{I}}{\boldsymbol{I_o}}\ \frac{p_0}{p}\right)\right]$$

I is a region of interest (ROI) within the Cu strip in the dark corrected raw radiograph. $\mathbf{I_o}$ is the same ROI positioned as in **I** but in the dark corrected background radiograph (Cu strip is absent). p is the mean of an ROI unobstructed by objects in the dark corrected raw radiograph. p_o is the mean of a ROI positioned as in p but in the dark corrected background radiograph. The ratio of p_o/p serves as a correction factor to the dark corrected background radiograph to account for changes in x-ray flux. Appendix A explores the individual components of $\mu_{Cu}L$ (i.e. mean of $\mathbf{I_o}$, mean of **I**, p_o, and p), illustrating distribution of values and line profiles.

5.1 Anomalously high values in $\mu_{Cu}L$ appear in the majority of scans after the 18th recorded scan at 160 kV

Figure 10 shows plots of $\mu_{Cu}L$ calculated for scan 2 and scan 30 at 160 kV. Elevated $\mu_{Cu}L$ values as illustrated in scan 30 appear after the eighteenth scan. As shown in Figure 11, there is no apparent pattern in location of the elevated $\mu_{Cu}L$ values in projections. Corresponding high values do not appear at 100 kV (Figure A1 in Appendix A). μ_{160kV} was examined as a function of number of spikes in $\mu_{Cu}L$ to determine any correlation. Figure 12 shows μ_{160kV} of water plotted as a function of number of spikes for 129 scans (blue dots) as well as the average value (black asterisks). While μ_{160kV} of water for a particular number of spikes varies, the average suggests a biasing of μ_{160kV} to higher values with increase number of spikes (at least for scans that contain 0-6 spikes as there are few scans with more than six spikes). When examining the ROI used to calculate **I** for projections with an elevated $\mu_{Cu}L$ value, no abnormally high single pixel values were found (not shown). As each projection is derived from the average of four frames, multi-frame data were acquired and evaluated to identify projections with elevated $\mu_{Cu}L$. As

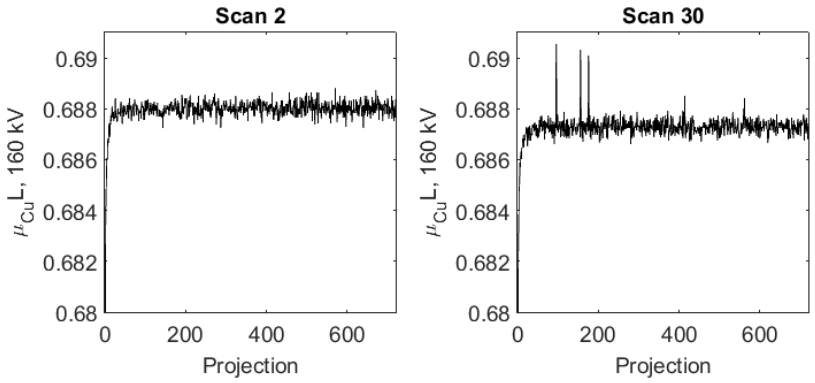

Figure 10 Plots of μ_{Cu}L for scan 2 and scan 30. Scan 30 illustrates three projections with elevated μ_{Cu}L values.

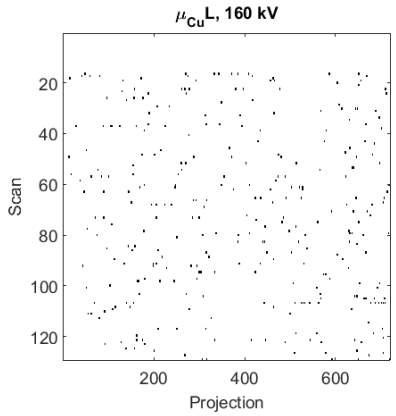

Figure 11 Plot showing scan and projection location of elevated μ_{Cu}L values for the first 129 scans.

shown in Figure 13, for projections with elevated μ_{Cu}L, the first frame demonstrates a 2% increase in the main section of the radiograph and 1% in the copper strip region. The spiking can then be attributed to abnormal values in the first frame only. The first frame was then excluded from the average, and projections were again reconstructed. No significant change was observed in μ (Figure 14). Scan 130 shows the most disagreement between the μ calculated from a three frame average compared to a four frame average for all materials. Upon examining the frames of the projections for scan 130, the first scan is observed to start when the carousel was still being translated. This is only observed in one of fourteen multi-frame data sets. While these anomalously high values in μ_{Cu}L are not desirable, they are not the dominating cause for drift. Still, these high values, however, may share a common cause with the drift.

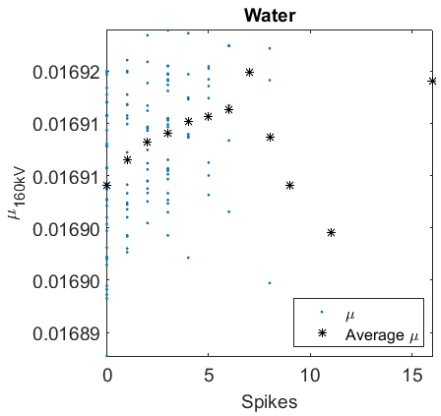

Figure 12 μ_{160kV} of water versus number of spikes in scan

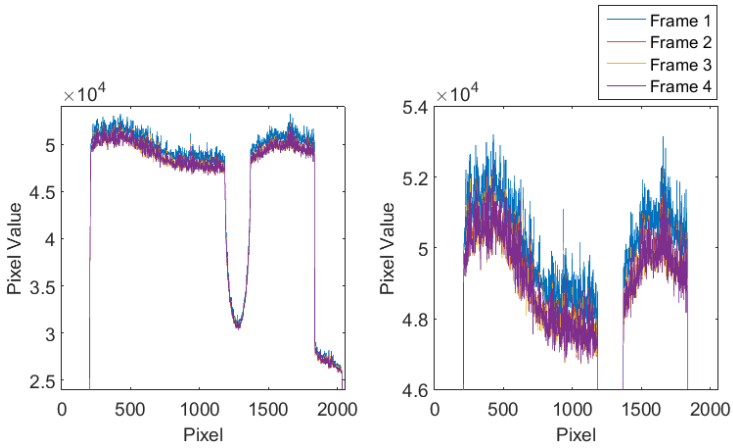

Figure 13 Individual frame line profiles centered in the upper slit of a projection which demonstrates an elevated frame.

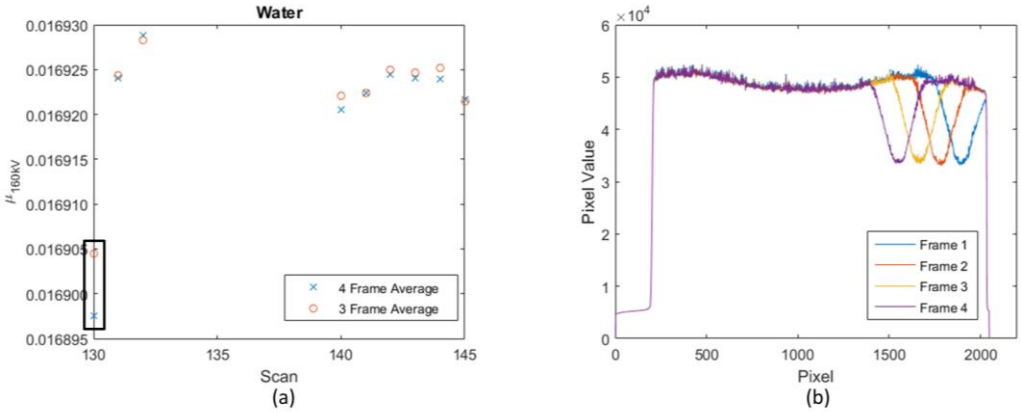

Figure 14 (a) Comparison of μ of water using a three frame average as oppose to a four frame average, and (b) four frames used in average of first projection for scan 130.

5.2 Scan at same power

It was hypothesized that the spikes may be caused by a difference of the power level at which the x-ray source operates. While comparing the x-ray source configurations at 100 kV and 160 kV, it was noted that at 100 kV the source was operated at a power output of 750 W and at 160 kV the source was operated at 1496 W. To evaluate the effect of this power difference on μ, the 160 kV protocol was modified by reducing the power by half (i.e. reducing mA by half) and doubling the integration time. Five scans were taken at the modified 160 kV protocol. Of the five scans, only one scan displayed one projection with elevated $\mu_{Cu}L$. As the change in protocol only increased the difference from the initial reference point, it was inconclusive as to whether this increased stability. Figure 15 updates the plot of μ as a function of scan to include these scans taken at this modified 160 kV protocol. Figure 16 shows μ^* plotted as a function of scan and demonstrates the correcting effect of normalizing by water at the energy of the scan.

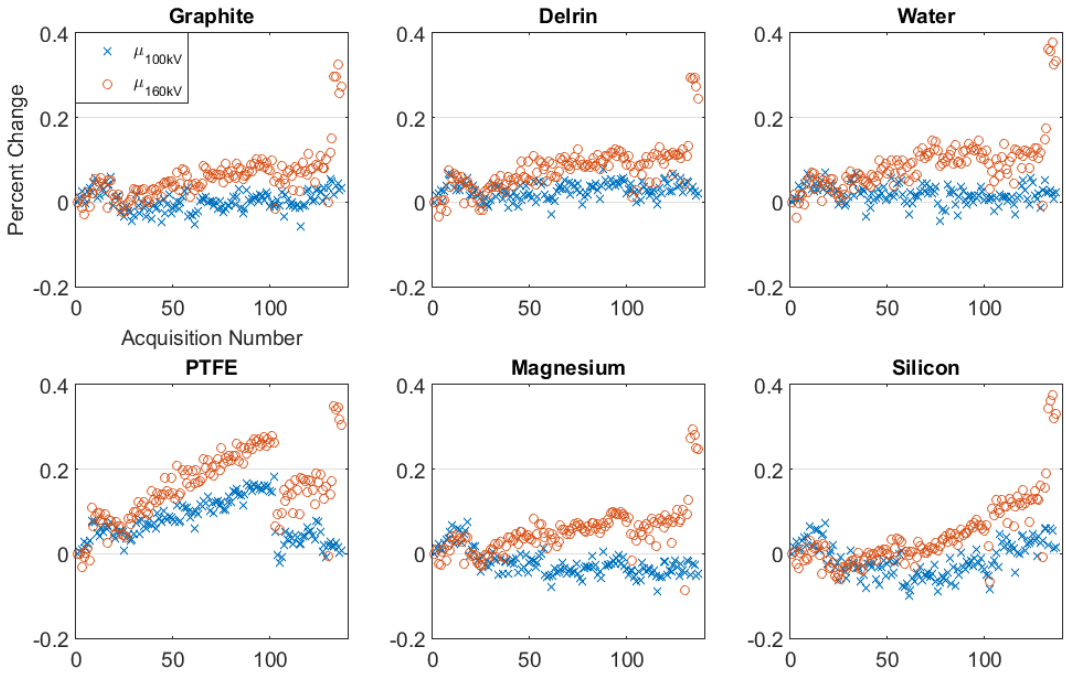

Figure 15 The percent change of μ at both 100 kV and 160 kV updated to include scans at the modified 160 kV protocol. PTFE data also includes data taken in assessing radiation effects for scans 104-130.

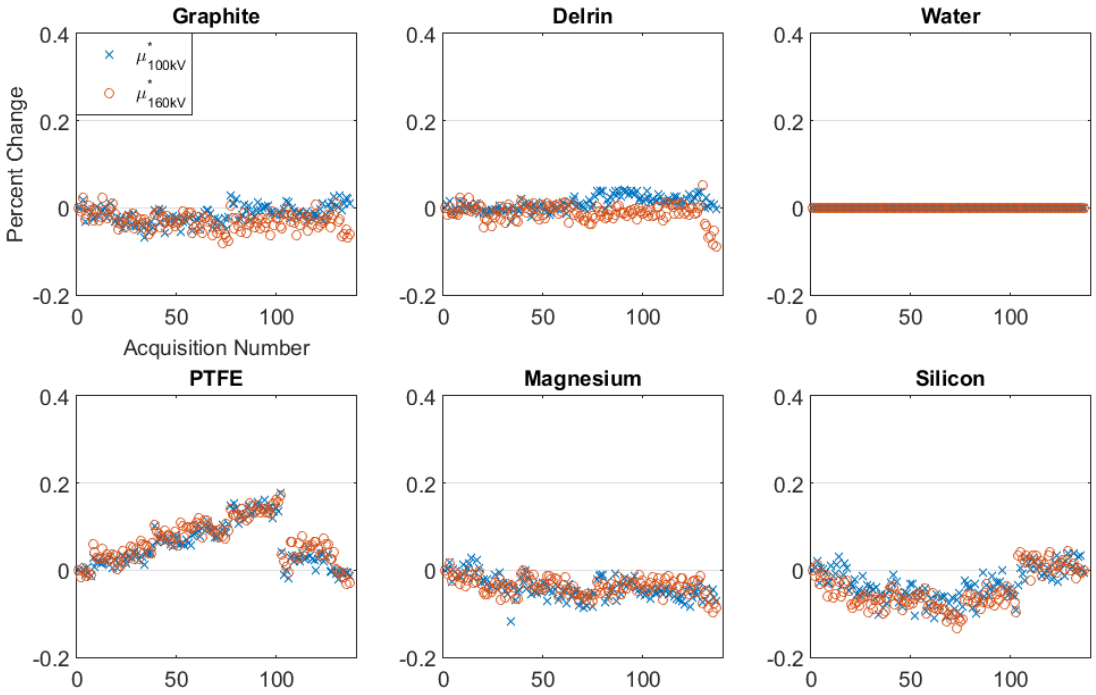

Figure 16 The percent change of μ^* in relation to the first scan at both 100 kV and 160 kV updated to include scans at the modified 160 kV protocol. PTFE data also includes data taken in accessing radiation effects for scans 104-130.

5.3 Trends in I, I_o, p, p_o

In Figure 17, note the relationship in trends between μ_{160kV} of water and the mean of **I** as a function of scan. The largest μ_{160kV} values correspond to the five measurements taken at the modified 160 kV protocol of half current, double integration time. It may be of interest to examine the effect of half current, same integration time as well as half integration time. We can then plot μ_{high} as a function of accumulated counts in mean of **I** divided by the integration time.

Since the largest μ_{160kV} values were taken under a different collection paradigm, they will be omitted in subsequent figures. Still, as illustrated in Figure 18, similar negative correlation is observed with all Cu strip parameters.

As illustrated in Figure 19, similar trends can be observed for graphite, Delrin, magnesium, silicon and water. PTFE behavior is probably influenced by radiation damage and the data set includes data taken when PTFE was being assessed for radiation degradation. Figure 20 compares the trends demonstrated by PTFE when data points taken during radiation testing are excluded. When those data points are excluded, the trend appears more linear. Correlation is not present at 100 kV (Figure 21). Further study is required to determine why there is no correlation at 100 kV.

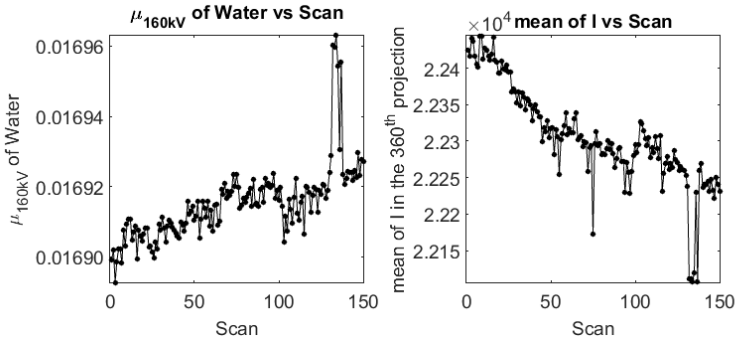

Figure 17 Plot of μ_{160kV} of water as a function of scan and plot of the mean of **I** in the 360th projection as a function of scan**.**

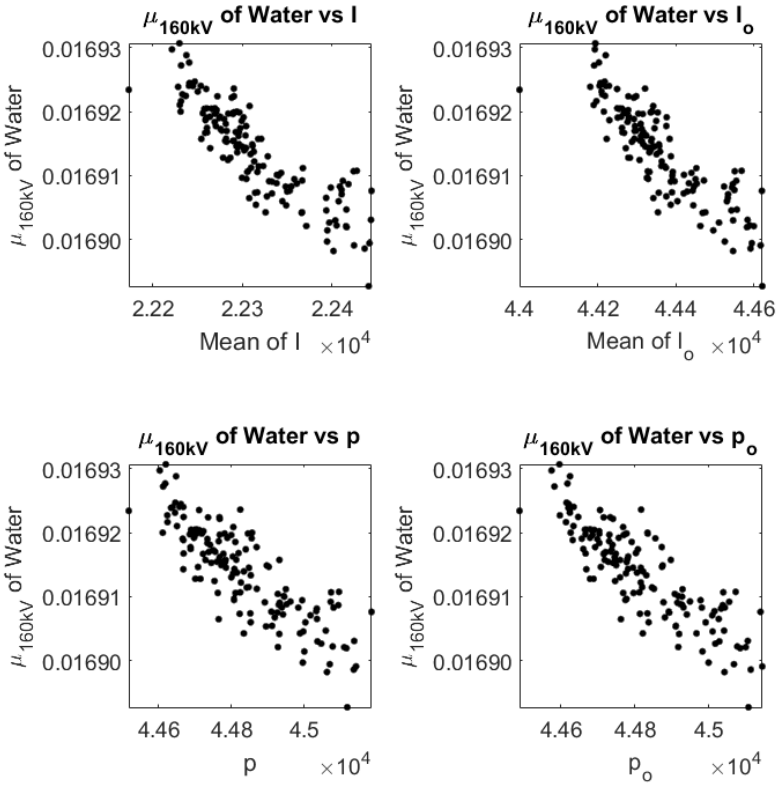

Figure 18 Plots of μ_{160kV} as a function of copper strip metric parameters (i.e. **I**, $\mathbf{I_o}$, p, p_o).

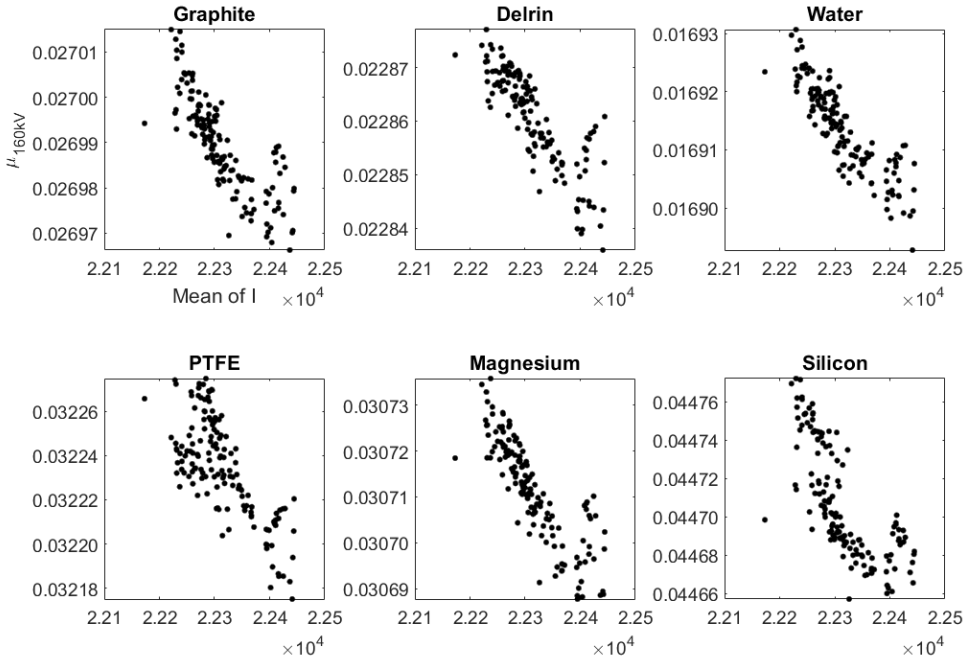

Figure 19 Plots of μ_{high} as a function of mean of **I** for the reference materials. PTFE data also includes data taken while assessing radiation effects during scans 104-130.

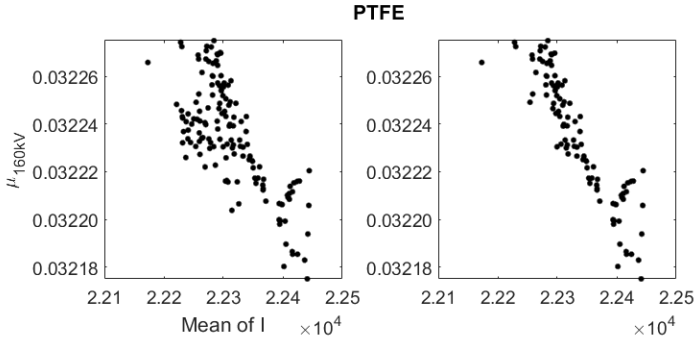

Figure 20 Comparison of μ_{160kV} as a function of the mean of **I** for PTFE. Left plot includes data points taken during radiation testing. Right plot excludes data points taken during radiation testing.

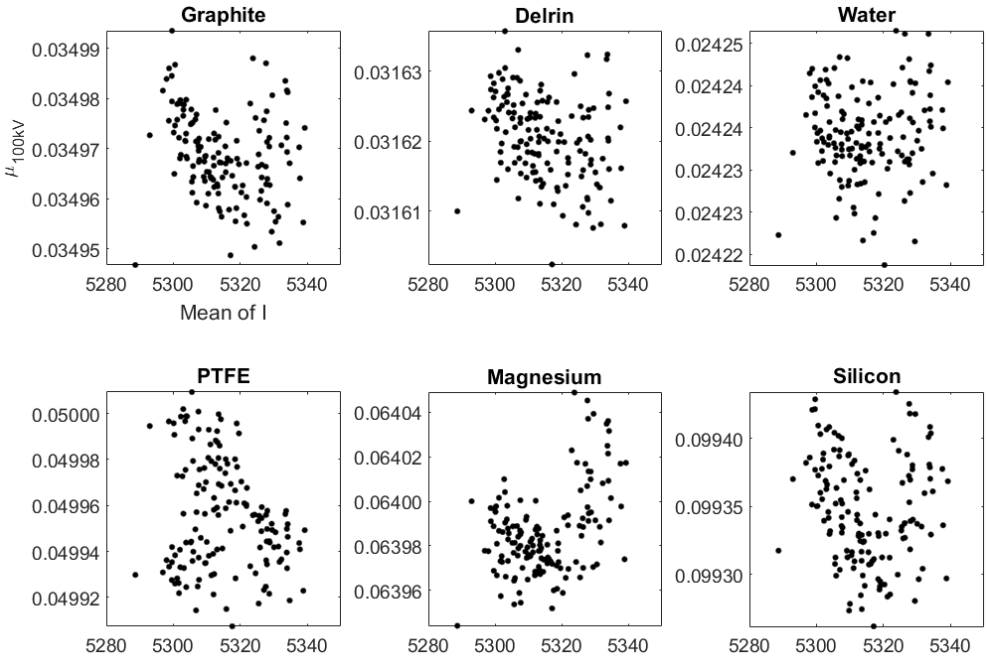

Figure 21 Plots of μ_{low} as a function of mean of **I** for the reference materials.

6. Evaluation of reconstruction postage stamp

As discussed in the introduction, radiographs are processed before reconstruction to produce *attenrads* following the equation:

$$attenrad = -\ln\left(\left[\frac{\boldsymbol{R_{raw}} - \boldsymbol{R_{dark}}}{\boldsymbol{R_{bak}} - \boldsymbol{R_{dark}}}\right]\frac{s_o}{s}\right)$$

Typically a reconstruction postage stamp is located on the upper strip for the purpose of normalizing for flux (Figure 22). Two variations were considered: (1) reconstruction with an alternative postage stamp region located in the lower strip and (2) reconstruction with the reconstruction postage stamp ratio set to 1. As illustrated in Figure 23, these changes to reconstruction did not change μ significantly enough to account for drift, suggesting that changes to flux during a scan are minimal. Given that no change in drift occurs when the reconstruction stamp ratio is set to 1, one can eliminate the reconstruction postage stamp as the cause of the drift.

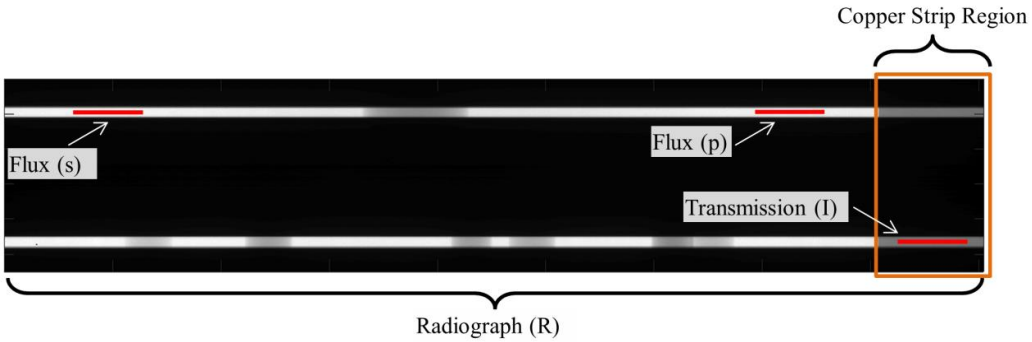

Figure 22 Sample raw radiograph illustrating location of parameters used to calculate the *attenrads* as well as Cu strip metric.

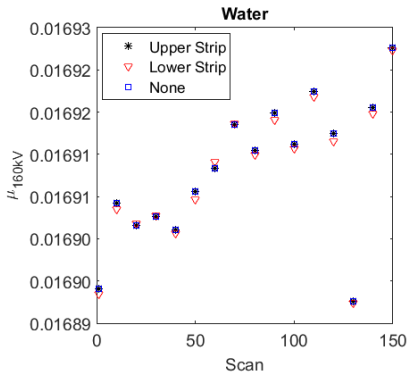

Figure 23 μ_{160kV} of water reconstructed with reconstruction postage stamp located in the upper strip (per standard protocol), lower strip and with reconstruction postage stamp ratio set to 1 (labeled as None).

7. Conclusion

Application requirements for studies performed on the MCT system at LLNL require accurate and precise μ values. As such the maximum allowable level of drift in μ was determined to be 0.1%. After ~100 scans were acquired during the period of November 2014 to March 2015, the drift in μ for the reference materials reached or exceeded 0.1%. The objective of this work was to identify strategies to account for and correct the drift. First, normalizing the 160 kV and 100 kV μ data by the μ of water at the corresponding energy significantly compensates for drift. It appears that PTFE undergoes radiation damage that alters μ. A promising alternative to PTFE is FEP, a material that has the same effective atomic number (Z_e) and electron density (ρ_e) as PTFE, but is 10 times more radiation resistant. This is important as effective atomic number and electron density are key parameters in analysis. The presence of a material with a Z_e and ρ_e like PTFE, when taken together with the remaining references, allows for a broad range of the (Z_e, ρ_e) feature space to be used in analysis. While FEP is documented as 10 times more radiation resistant, testing will be necessary to assess how often, if necessary, FEP will need to be replaced. FEP rods have been acquired and are ready for evaluation. Analysis of the Cu strip metric showed an inverse correlation between radiograph pixel values and μ_{160kV} of the reference values. Correlation is not observed at 100 kV. Further measurements are necessary to elucidate the mechanism driving the correlation at 160 kV.

Glossary of Terms

I	Region of interest (ROI) within the Cu strip in the dark corrected raw radiograph
$\mathbf{I_o}$	Same ROI positioned as in **I** but in the dark corrected background radiograph (Cu strip is absent).
MCT	Micro-Computed Tomography
p	Mean intensity for an ROI unobstructed by objects in the dark corrected raw radiograph
p_o	Mean of a ROI positioned as in *p* but in the dark corrected background radiograph
$\mathbf{R_{dark}}$	Dark radiograph
$\mathbf{R_{raw}}$	Raw radiogrpah
$\mathbf{R_{bak}}$	Background radiograph
S	Mean of an ROI unobstructed by objects in the dark corrected raw radiograph
S_o	Mean of an ROI positioned as in s, but in the dark corrected background radiograph
μ	Linear attenuation coefficient, in units of mm^{-1}.
μ'	Linear attenuation coefficient normalized by the linear attenuation coefficient of water at the corresponding energy.
$\mu_{Cu}L$	Copper strip metric

Appendix A: Cu Strip Analysis

The Copper strip metric can be written as

$$\mu_{Cu}L = mean\left[-\ln\left(\frac{\boldsymbol{I}}{\boldsymbol{I_o}}\ \frac{p_0}{p}\right)\right] = mean\left[\ln\left(\frac{\boldsymbol{I_o}}{\boldsymbol{I}}\right)\right] + \ln\left(\frac{p}{p_o}\right) = mean(T) + C$$

The plots that follow characterize the distributions of μ_{Cu}L, T, C. The individual components of T and C (i.e. I_o, I, p_o, and p) are also examined.

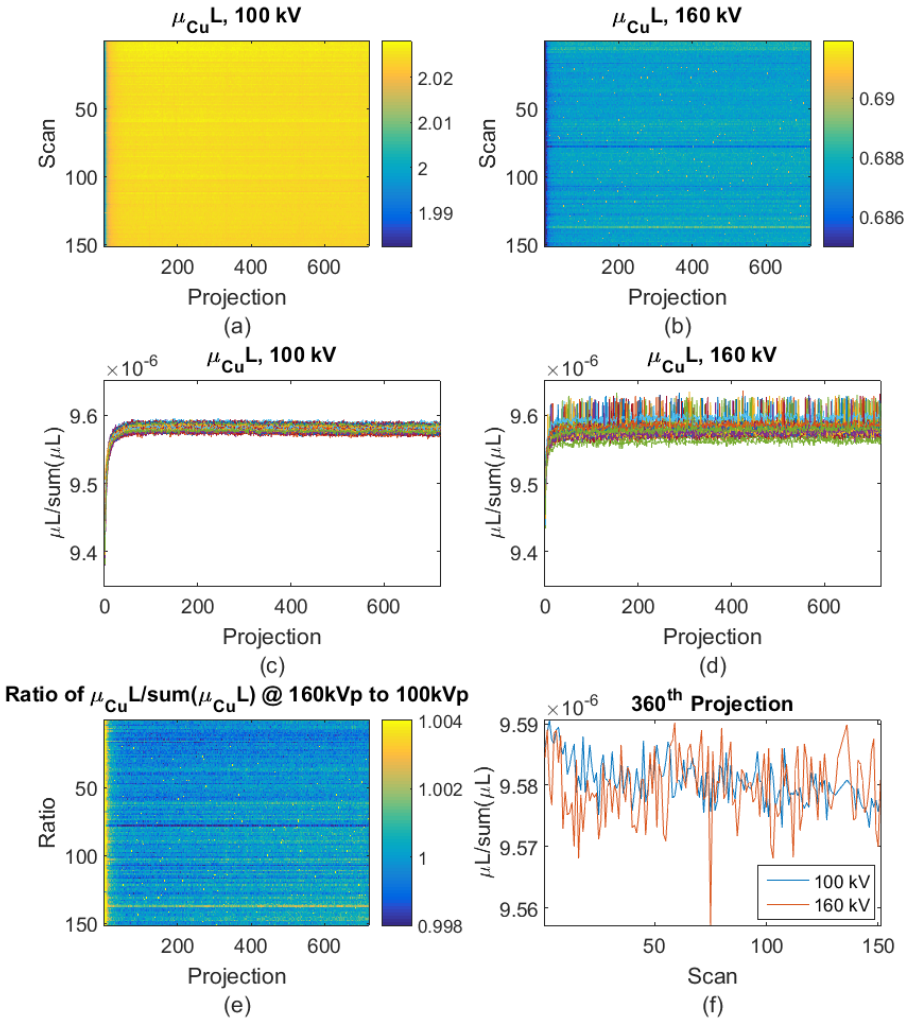

Figure A1 Characterization of $\mu_{Cu}L$. 2D plot of $\mu_{Cu}L$ for 720 projections and 150 scans acquired at (**a**) 100 kVp and (**b**) 160 kVp. To compare distributions, projection data from (**a**) and (**b**) are divided by the sum of all projections from all scan at a specified energy. This adjusted $\mu_{Cu}L$ is plotted for all scans in (**c**) for 100 kVp and (**d**) for 160 kVp. The ratio of the adjusted projection data is shown in (**e**). The adjusted $\mu_{Cu}L$ at the 360th projection as a function of scan is shown in (**f**).

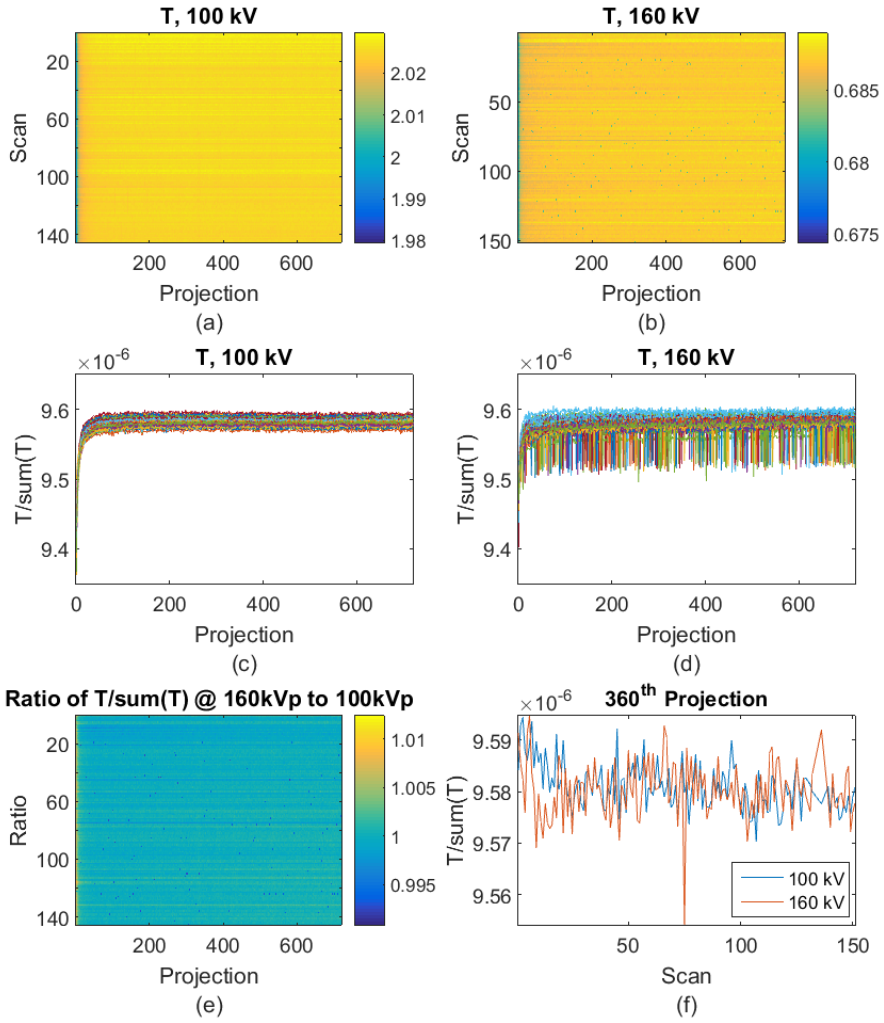

Figure A2 Characterization of *T*. 2D plot of *T* for 720 projections and 150 scans acquired at (**a**) 100 kVp and (**b**) 160 kVp. To compare distributions, *T* from (**a**) and (**b**) are divided by the sum of all projections for all scans at a specified energy. This adjusted *T* is plotted for all scans in (**c**) for 100 kVp and (**d**) for 160 kVp. The ratio of the adjusted *T* is shown in (**e**). The adjusted *T* at the 360th projection as a function of scan is shown in (**f**).

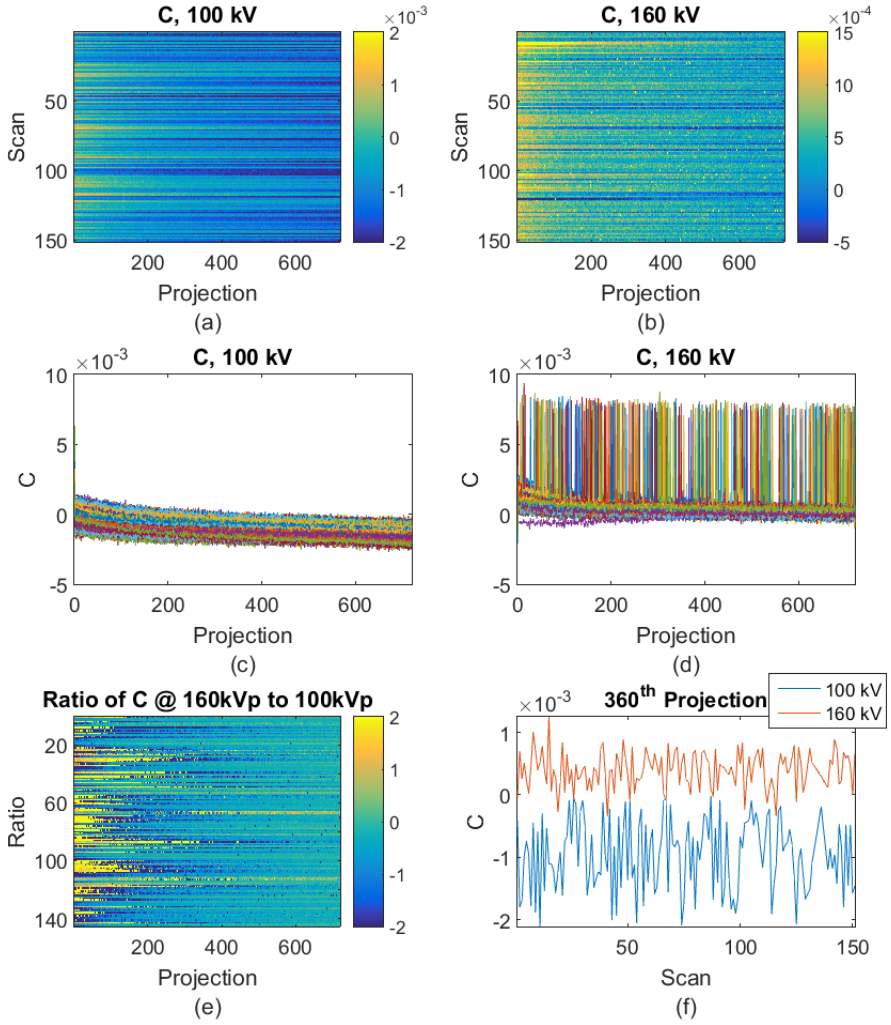

Figure A3 Characterization of *C*. 2D plot of *C* for 720 projections and 150 scans acquired at (**a**) 100 kVp and (**b**) 160 kVp. *C* is plotted for all scans in (**c**) for 100 kVp and (**d**) for 160 kVp. The ratio of *C* at 160 kVp to 100 kVp is shown in (**e**). *C* at the 360th projection as a function of scan is shown in (**f**).

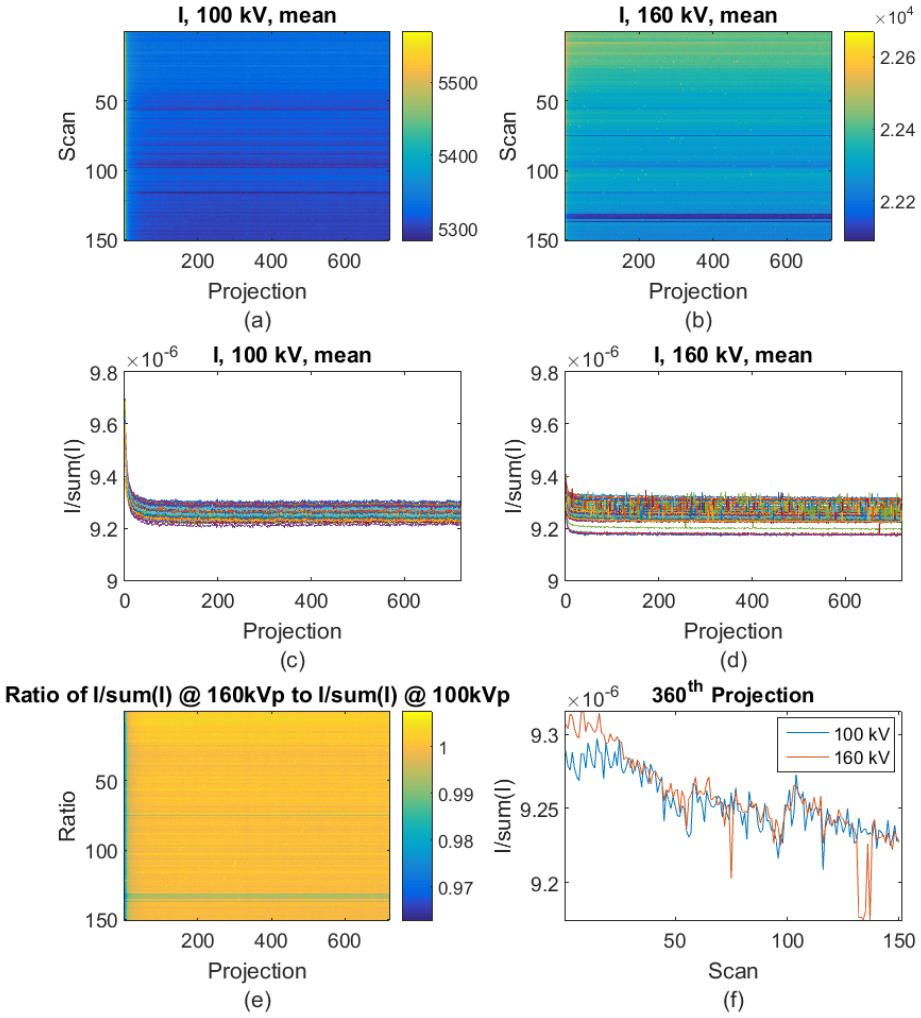

Figure A4 Characterization of *I*. 2D plot of *I* for 720 projections and 150 scans acquired at (**a**) 100 kVp and (**b**) 160 kVp. To compare distributions, *I* from (**a**) and (**b**) are divided by the sum of all *I* for all projections and all scans at a specified energy. This adjusted *I* is plotted for all scans in (**c**) for 100 kVp and (**d**) for 160 kVp. The ratio of the adjusted *I* at 160 kVp to 100kVp is shown in (**e**). The adjusted *I* at the 360th projection as a function of scan is shown in (**f**).

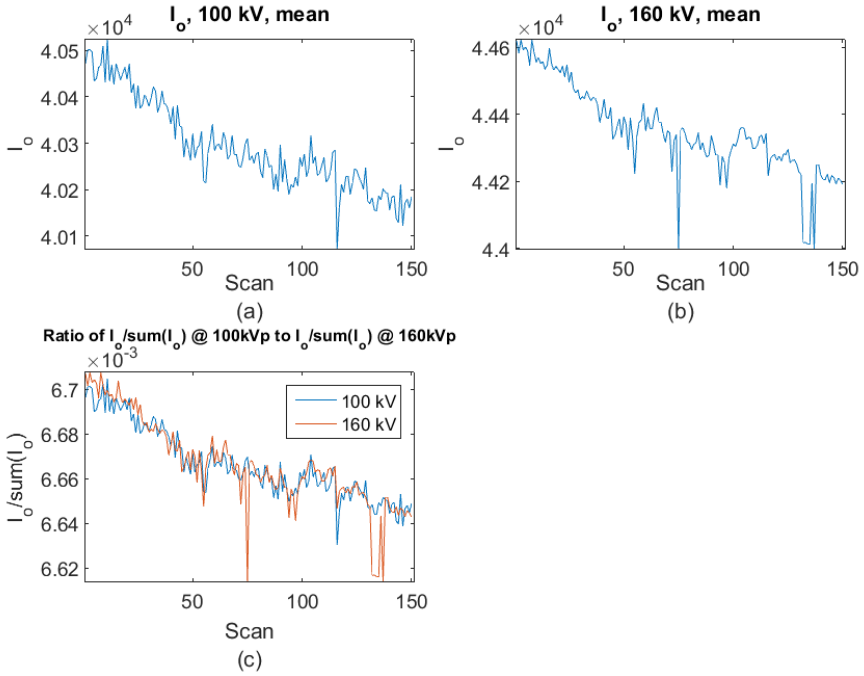

Figure A5 Characterization of I_o. I_o plotted for all scans in (**a**) for 100 kVp and (**b**) for 160 kVp. To compare distributions, I_o from (**a**) and (**b**) are divided by the sum of all I_o for all scans at a specified energy and plotted in (**c**).

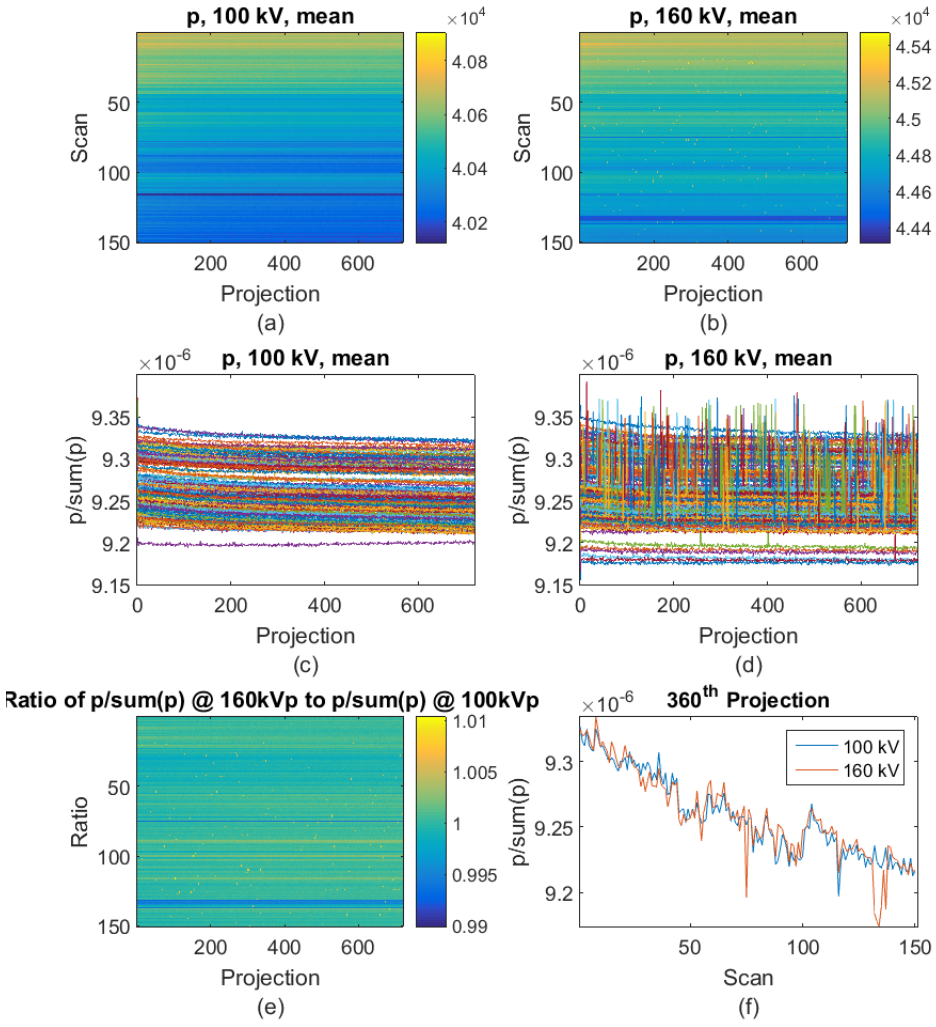

Figure A6 Characterization of *p*. 2D plot of *p* for 720 projections and 150 scans acquired at (**a**) 100 kVp and (**b**) 160 kVp. To compare distributions, *p* from (**a**) and (**b**) are divided by the sum of all *p* for all projections and all scans at a specified energy. This adjusted *p* is plotted for all scans in (**c**) for 100 kVp and (**d**) for 160 kVp. The ratio of the adjusted *p* at 160 kVp to 100kVp is shown in (**e**). The adjusted *p* at the 360th projection as a function of scan is shown in (**f**).

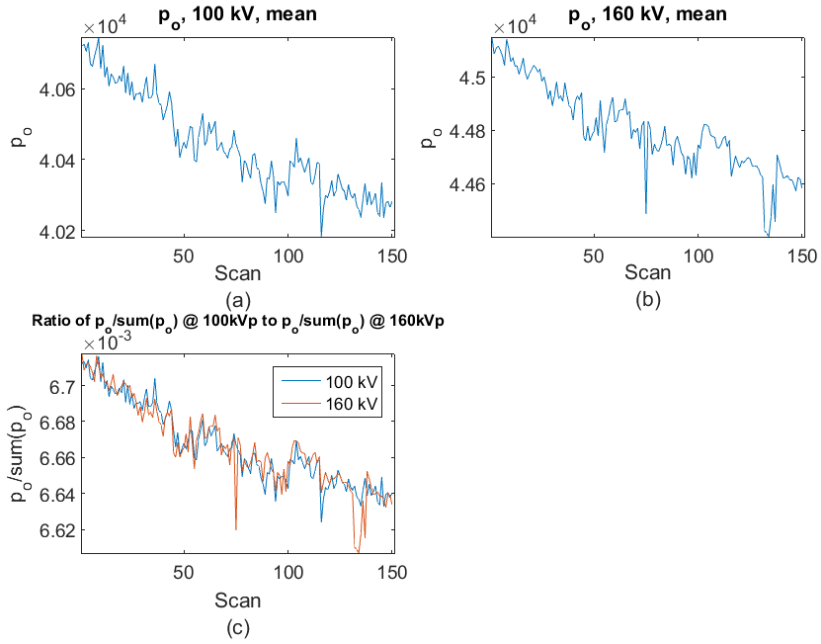

Figure A7 Characterization of p_o. p_o plotted for all scans in (**a**) for 100 kVp and (**b**) for 160 kVp. To compare distributions, p_o from (**a**) and (**b**) are divided by the sum of all p_o for all scans at a specified energy and plotted in (**c**).

Disclaimer and Auspices

This work performed under the auspices of the U.S. Department of Energy by Lawrence Livermore National Laboratory under Contract DE-AC52-07NA27344. Pursuant to Section 309(a)(1)(c) of the Homeland Security Act of 2002 (Public Law 107-296) that authorizes the DHS to task DOE national laboratories on a "work for others" basis.

References

BROWN, W. & SMITH, J. 2013. Documentation of the ISA Micro Computed Tomography System.

JOHNSON, T. R., KRAUSS, B., SEDLMAIR, M., GRASRUCK, M., BRUDER, H., MORHARD, D., FINK, C., WECKBACH, S., LENHARD, M., SCHMIDT, B., FLOHR, T., REISER, M. F. & BECKER, C. R. 2007. Material differentiation by dual energy CT: initial experience. *Eur Radiol,* 17**,** 1510-7.

LENNOX, K. P., AUFDERHEIDE, M., WHITE III, W. T., ROBERSON, P., SMITH, J. A. & GLASCOE, L. G. 2014. HADES Single-Ray Model Validation.

NISHIOKA, A., MATSUMAE, K., WATANABE, M., TAJIMA, M. & OWAKI, M. 1959. Effects of gamma radiation on some physical properties of polytetrafluoroethylene resin. *Journal of Applied Polymer Science,* 2.

SEETHO, I., BROWN, W., KALLMAN, J., MARTZ, H. & WHITE, W. T. 2011. MicroCT: Automated Analysis of CT Reconstructed Data of Home Made Explosive Materials Using the Matlab MicroCT Analysis GUI.

STERIGENICS Datasheet: Material Considerations Irradiation Processes.